Research Article | Vol. 27, No. 11 | 27 May 2019 | OPTICS EXPRESS 16395
Optics EXPRESS

Convective Nozaki-Bekki holes in a long cavity OCT laser

SVETLANA SLEPNEVA,[1,2,3,*] BEN O'SHAUGHNESSY,[2,3] ANDREI G. VLADIMIROV,[4,5] SERGIO RICA,[6,7] EVGENY A. VIKTOROV,[8] AND GUILLAUME HUYET[1]

[1] *Université Côte d'Azur, CNRS, INPHINY, France*
[2] *Centre for Advanced Photonics and Process Analysis & Department of Physical Sciences, Cork Institute of Technology, Cork, Ireland*
[3] *Tyndall National Institute, University College Cork, Lee Maltings, Dyke Parade, Cork, Ireland*
[4] *Weierstrass Institute, Mohrenstr 39, Berlin, Germany*
[5] *Lobachevsky State University of Nizhny Novgorod, 23 Gagarina av., 603950 Nizhny Novgorod, Russia*
[6] *Facultad de Ingeniería y Ciencias, Universidad Adolfo Ibáñez, Santiago, Chile*
[7] *UAI Physics Center, Universidad Adolfo Ibáñez, Santiago, Chile*
[8] *ITMO University, Saint Petersburg, Russia*
[*] *svetlana.slepneva@gmail.com*

Abstract: We show, both experimentally and theoretically, that the loss of coherence of a long cavity optical coherence tomography (OCT) laser can be described as a transition from laminar to turbulent flows. We demonstrate that in this strongly dissipative system, the transition happens either via an absolute or a convective instability depending on the laser parameters. In the latter case, the transition occurs via formation of localised structures in the laminar regime, which trigger the formation of growing and drifting puffs of turbulence. Experimentally, we demonstrate that these turbulent bursts are seeded by appearance of Nozaki-Bekki holes, characterised by the zero field amplitude and π phase jumps. Our experimental results are supported with numerical simulations based on the delay differential equations model.

1. Introduction

OCT is a powerful imaging technique that enables the acquisition of real-time images of scattering media that are semi-transparent in the near-infrared range [1]. While OCT initially relied on white light interferometry using low coherence superluminescent diodes, new techniques such as swept-source OCT (SS-OCT) enable the realisation of 3D-real-time video of biological tissues [2]. In SS-OCT, the image quality depends on the property of a swept source, which is a laser whose output wavelength is periodically modulated [3]. For example, the axial resolution is inversely proportional to the width of the optical spectrum while the image depth is limited by the coherence length. This coherence length, which can be measured by a conventional interferometric technique or by a more complex direct measurement of the electric field [4], is limited by various physical phenomena ranging from mode-hopping [5], parasitic noise source [6], cavity dispersion [7] or, more generally, by the appearance of instabilities. In this paper, we study coherence properties of a long SS-OCT laser and find out that the mechanism leading to the loss of coherence is similar to the laminar-turbulent transition in hydrodynamic flows.

The laminar-turbulent transition [8,9] is a crucial problem of engineering and science motivated by many applications such as turbulent transport, atmospheric flows and airplane development while remaining a partially understood problem of fluid dynamics [10, 11]. The transition from laminar to turbulent flow follows usually the same scenario, evolving from a stationary motion to well-defined oscillations eventually ending in a turbulent wake. For example, the Poiseuille flow inside a pipeline demonstrates an interesting example of the transition to turbulence since

#348383 https://doi.org/10.1364/OE.27.016395
Journal © 2019 Received 25 Oct 2018; revised 26 Mar 2019; accepted 1 Apr 2019; published 24 May 2019

Optics EXPRESS

the laminar flow is theoretically linearly stable for any speed [12] (or Reynolds number) but experimental observations show the development of turbulence associated with the formation of a turbulent spot downstream indicating that a finite amplitude perturbation destabilises the laminar regime [9].

The important role of nonlinearities was first understood phenomenologically in the 1950s after the pioneering work of L. D. Landau [13]. The transition from a laminar to a turbulent state may be characterized by the notion of bifurcation which has been at the centre of important developments from the 60s up to the present [14]. Many features observed in a turbulent flow are closely connected to the formation of localised structures such as solitary waves or vortices. These structures are naturally observed in nonlinear optics [15, 16], which has become an excellent test-bed to investigate turbulence and the emergence of complexity in spatially extended systems [17]. It was, for example, suggested that the transition to turbulence in a long cavity laser could be explained in the frame of a nearly conservative system where the balance between dispersion and Kerr nonlinearities leads to dark and grey soliton clustering [18]. Rogue waves [19] and turbulent puffs in the transition to turbulence [20] have also been observed in polarisation dynamics of partially mode-locked and quasi-CW lasers.

Here, we demonstrate that the transition from laminar to turbulence can occur in a long laser operating at the zero dispersion point. In addition to dissipative saturable nonlinearities, our laser system includes a tunable spectral filter. The spectral filtering is equivalent to diffusion within the framework of the complex-Ginzburg Landau equation [21]. If the filter is driven in near resonance with the cavity round trip time, we observed and analysed the transition between absolute and convective instabilities. In the convective instability regime, we show that turbulent puffs, generated by localised structures, seed the growth of turbulence leading to de-coherence of the laser field. Convective instabilities are commonly observed in open flow instabilities where a disturbance may grow in time as it travels away from the region of its birth so its amplitude grows at any point along the path before eventually decaying to its original value. This contrasts with the more conventional absolute instabilities where an initial disturbance spreads out along the entire unstable region [22–25]. In the convective regime, noise-induced spots, swirls and other structures are commonly observed in hydrodynamic turbulence. Noise may also lead to the appearance of a laminar-turbulent transition at finite distance in the convective regime as demonstrated by Deissler [26]. Turbulent puffs in the transition to turbulence have also been observed in partially mode-locked laser [20] and associated with the formation of rogue waves. In our case, turbulent puffs are generated by Nozaki-Bekki holes which we observed experimentally and analyzed in the frame of delay differential equations.

2. Experimental setup and theoretical model

Our experimental setup consisted of a long cavity swept laser which incorporated a semiconductor amplifier as a gain medium and a narrow bandwidth (50pm) Fabry-Pérot tunable filter. The optical output of the laser was following the central frequency of the filter ($\Delta(t)$) generating wavelength sweeps of several nm around the 1300nm central wavelength. The temporal evolution of the output power was studied by coupling the laser light to a high speed photodetector and further analysed on a 12GHz real-time oscilloscope. The laser cavity had a length of about 20m. In this case, the laser was operating in a quasi-static regime meaning the frequency of the wavelength sweep was in the order of 1Hz.

Theoretically, we analysed the system using the following delayed differential equations that describe the temporal evolution of the laser gain $G(t)$ and the electric field envelope $A(t)$ as in [27]. These equations read

$$\dot{A}(t) + (\Gamma - i\Delta(t))\, A(t) = \Gamma\sqrt{\kappa} e^{(1-i\alpha)G(t-T)/2} A(t-T), \tag{1}$$

$$\dot{G}(t) = \gamma \left[g_0 - G(t) - \left(e^{G(t)} - 1 \right) |A(t)|^2 \right], \tag{2}$$

Optics EXPRESS

where $\dot{A}(t)$ and $\dot{G}(t)$ are the time derivatives of the electric field envelope and the laser gain, T is the delay time, corresponding to the roundtrip time of the light in the cavity, g_0, γ, α, Γ and κ are the unsaturated gain, gain relaxation rate, linewidth enhancement factor, filter width and attenuation factor per roundtrip from cavity losses, respectively.

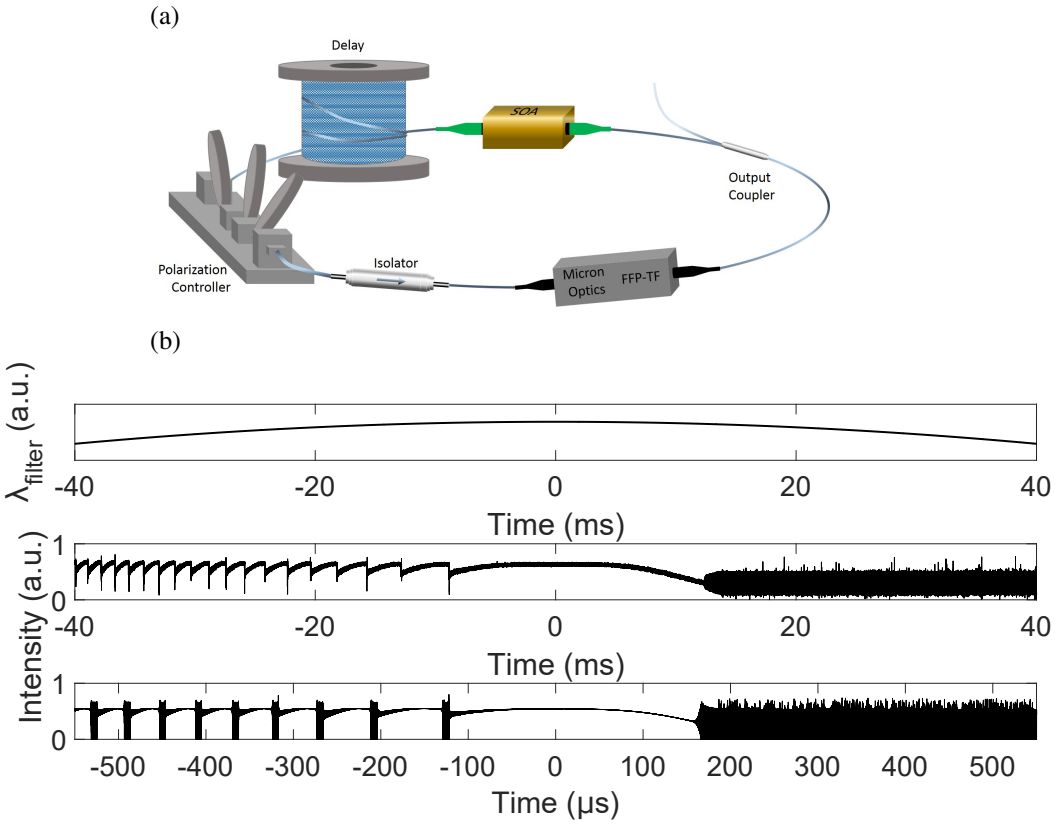

Fig. 1. Subcritical and supercritical bifurcations in a wavelength swept laser. (a) Experimental set-up of a long cavity wavelength swept laser incorporating a semiconductor optical amplifier (SOA) and a fast Fabry-Pérot tunable filter (FFP-TF) (see the detailed description of the laser components in [27]). (b) The filter wavelength variation in time (top). Experimental (middle) and theoretical (bottom) observations of subcritical and supercritical modulational instabilities. A sequence of subcritical bifurcations occurs as the filter transmission wavelength increases while a single supercritical bifurcation leads to the appearance of a turbulent state as the the filter transmission wavelength decreases. The experimental time trace was recorded for the laser with a 20m cavity length and 1Hz filter modulation frequency. The theoretical time trace was obtained by direct numerical simulation of Eqs. (1) and (2) with a cavity round trip time of 14ns.

When the filter moved in a low sweep rate regime, we observed both experimentally and theoretically, that the single mode laser operation underwent either a subcritical or a supercritical Hopf bifurcation depending on the direction of the filter tuning as described in [27]. The increase of the filter transmission wavelength resulted in a subcritical bifurcation that ultimately led to the transition to another, red-detuned, single mode operation. The decrease of the filter transmission wavelength resulted in a supercritical bifurcation which led to the emergence of a turbulent regime. Such behaviour, as illustrated in Fig. 1(b), was observed when the filter wavelength was periodically modulated at a very low frequency (less than 10Hz).

Optics EXPRESS

Next, the laser was set to operate in a Fourier Domain Mode-Locked (FDML) regime [28]. This regime is achieved by adding extra single mode fiber delay into the cavity and increasing the cavity length up to 20km. In this case it was possible to synchronise the period of the filter modulation (T_F) with the roundtrip time of the light in the cavity (T). An interpretation of the phase shift introduced by dynamically tuned Fabry-Pérot filter with the help of Doppler effect is given in [29, 30]. In this regime, the sweeping rate was in the order of 10kHz. Interestingly, the motivation to investigate the dynamics of FDML lasers is mostly driven by its application in SS-OCT [1, 2, 31] and more recently, Raman spectroscopy [32]. This laser, due to its unprecedented high sweep rates, enables volumetric video-rate real time OCT imaging whose quality relies on ultra-fast broadband swept sources with a long coherence length. However the loss of coherence within the sweep leads to deterioration of the image quality and limits the generation of extremely short pulses to 60ps after optical decompression [33].

The bifurcation analysis of the FDML laser reveals similar regimes as described in the case of a low sweep rate laser [27]. In order to relate the evolution of the FDML output to the turbulent behaviour commonly observed in spatio-temporal systems, we reconstructed space-time diagrams of the laser intensity in analogy with [34].

Experimentally, this was carried out by recording the laser output during a small time window of length t_W ($t_W \ll T$), repeated with a period matching the filter sweep period T_F. For each filter sweep number n, we examined the intensity of the laser in the interval $nT_F < t < nT_F + t_W$. The electric field was then treated as a function of two variables: time and filter period number n. A 2D picture of the laser dynamics is thus created for a small part of the filter sweep.

In our theoretical simulations, we followed a similar approach, integrating in the limit of a very large delay near the bifurcation point. The experimental realisation of the FDML regime required a very long cavity length. The delay differential equation model could be used to run simulations of this laser but the delay would be very large, requiring lots of computation. The dynamics of interest are in a small time window where laminar flow drifts into a region of instability and becomes turbulent over many sweep periods. The simplest case is close to the filter turning point, where the filter moves slowly and the laminar flow is a single mode solution to the delayed differential equations model, instead of a chirped FDML solution. By using the analytical solution for the laminar part and by assuming the cavity roundtrip time to be arbitrarily long, we can simulate only the required portion of each filter sweep (Table 1).

Table 1. Parameter values for simulations

Parameter	Description	Value
γ	Carrier relaxation rate	4GHz
κ	Linear attenuation factor	0.04
α	Linewidth enhancement factor	5.0
g_0	Unsaturated gain per roundtrip	5.0
$\pi\Gamma$	Filter full width at half maximum	9GHz

The electric field during the nth sweep is $A_n(t) = A(t + nT_F)$. We consider the case where $T = T_F + \tau$, with $\tau > 0$, so that the electric field drifts in the positive t direction relative to the filter sweep profile with each subsequent period. In order to simulate $A_n(t)$ in the time window $0 < t < t_W$, the required delayed term is given by $A_{n-1}(t)$, with the time window offset by τ as shown in Fig. 2. For $t > 0$ this history comes from previous simulation or initial conditions. We assume that the filter is static at zero frequency for an arbitrarily long time before $t = 0$ so that a

Optics EXPRESS

single mode solution can be calculated analytically in this region, filling in the history for $t < 0$.

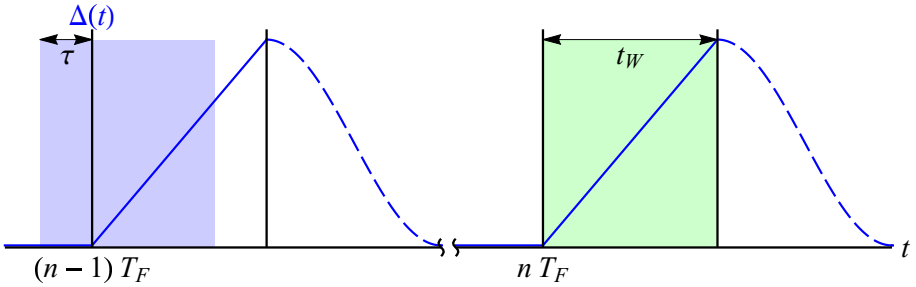

Fig. 2. Plot of filter sweep profile, $\Delta(t)$, used for simulations. For each sweep period n the model equations are numerically integrated in the green shaded region using the delayed term from the blue shaded region. The solution in the region where $\Delta(t) = 0$ is calculated analytically and the dashed region where the filter returns to zero is ignored.

The full filter sweep used for simulation is as follows. The filter starts at frequency f_0 at $t = 0$ and decreases linearly during the simulated time interval. After the simulated interval the filter returns to f_0 and remains there for the remainder of the arbitrarily long filter sweep, allowing the system to return to single mode operation before the beginning of the next simulated interval. The filter sweep profile of the real laser follows a sine wave. Near the turning point the filter is almost static for a time which is long compared with the time scale of the laser dynamics.

There is some equivalence between the single mode operation and chirped FDML operation. The following transformation puts the system in a frame where the filter is always at zero frequency, $A(t) = a(t) \exp\left(i \int_{t-T}^{t} \Delta(t')dt'\right)$. If the filter period is perfectly tuned to match the cavity round trip time then this system is identical to a system with a static filter, but the single mode solutions in this "filter frame" system correspond to chirped FDML solutions. In the case of small detuning these solutions drift away from the filter over many round trips. Laminar FDML thus has similar instabilities to single mode operation, so a study of the single mode case provides insight into the transition to turbulence in FDML.

3. Nozaki-Bekki holes

When the filter was driven in a perfect resonance with the cavity roundtrip time, the laser emitted a set of frequency modulated outputs corresponding to single modes in the filter frame [27]. These modes have the same stability criteria as the modes observed when the central frequency of the filter is fixed. When the filter was tuned out of resonance from the cavity round trip, the stability of these frequency modulated outputs depended on detuning $\delta = 2\pi(1/T_F - 1/T)$. While the behaviour of the supercritical bifurcation remained qualitatively the same for any values of δ, the dynamics around the subcritical point strongly depended on its value and, to investigate this point further, we considered the dynamics for the increasing values of $\delta > 0$. As δ increased, we identified four different regimes. For $\delta < \delta_{c_1}$, the laminar regime remained stable for the entire sweep. For $\delta_{c_1} < \delta < \delta_{c_2}$, the laminar regime became turbulent as soon as it passed the bifurcation point; the transition between laminar and turbulent regimes remained at a fixed value of the filter frequency. This regime is consistent with an absolute instability as illustrated by 2D diagrams in Figs. 3(a) and 4(a) (experimental) and Figs. 3(b) and 4(b) (theoretical).

For the larger detuning values, *i.e.* $\delta_{c_2} < \delta < \delta_{c_3}$, the laminar regime invaded the turbulent regime at a rate much faster than the growth rate of the turbulent regime (Figs. 3(c) and 4(c) (experimental) and Figs. 3(d) and 4(d) (theoretical)). In this case, the front between the laminar and turbulent regimes was no longer synchronised with the filter position but returned at every roundtrip time. In the filter frame this appeared as a front drifting with a "speed" proportional to

Optics EXPRESS

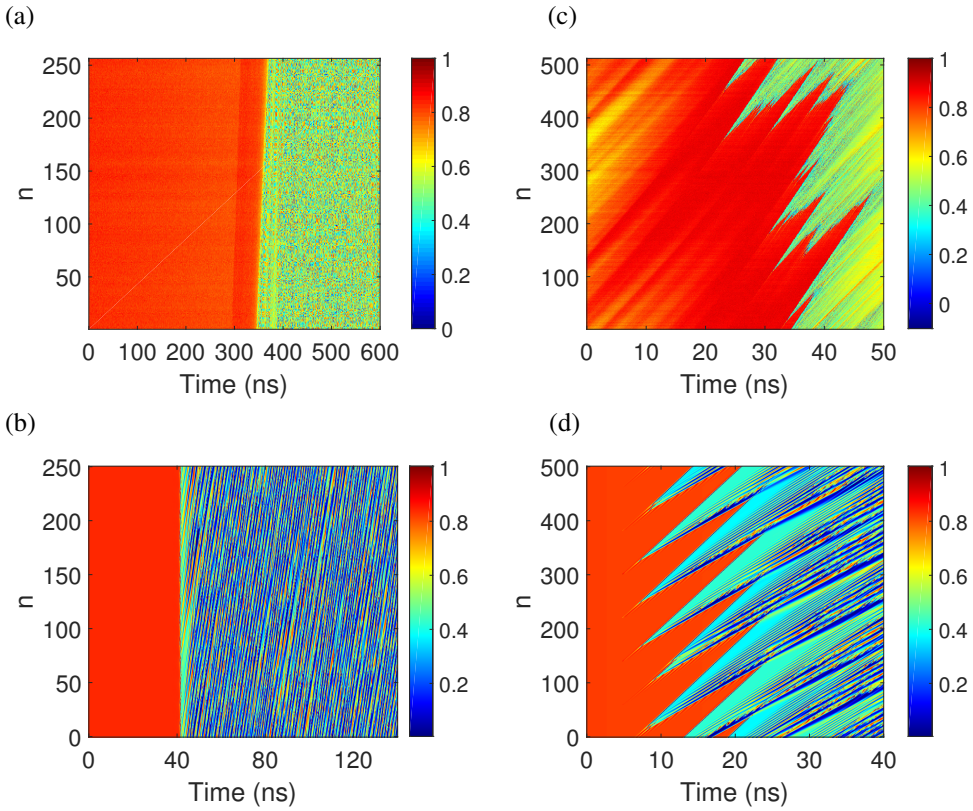

Fig. 3. Evolution of the laser intensity near the transition between the laminar and turbulent regimes for subsequent filter periods (n). Experimental (a) and theoretical (b) 2D diagrams of the laser intensity evolution for 250 subsequent roundtrips in the absolute instability regime corresponding to $\delta_{c_1} < \delta < \delta_{c_2}$. Experimental (c) and theoretical (d) 2D diagrams of the laser intensity evolution for the subsequent 500 roundtrips in the convective instability regime corresponding to $\delta_{c_2} < \delta < \delta_{c_3}$. The triangular features in (c) and (d) represent the emergence of localised structures from the laminar regime. These structures drift toward the turbulent region with a speed $v \sim 1/p_{up}$ and the size of the turbulent spot grows at a rate $r \sim 1/p_{low} - 1/p_{up}$, where p_{up} and p_{low} are the slopes of the upper and lower boundaries between the laminar state and the localised structures. The colorbars represent the normalised laser intensity. The parameters for simulations are given in Table 1.

the detuning. As the laminar regime invaded the turbulent region, we observed spontaneous noise induced creation of turbulent puffs which were mediated by the formation of spatio-temporal topological defects. For $\delta_{c_3} < \delta$, the laser displayed a turbulent regime throughout the entire sweep. Experimentally, the values for δ_{c_1}, δ_{c_2} were found to be on the order of a few mHz while δ_{c_3} was on the order of a few hundreds of mHz. The values of detuning below δ_{c_1} are the most promising for the imaging applications, yet difficult to achieve experimentally [29].

The temporal evolution of the laser intensity near the subcritical bifurcation point as a function of the filter period number n is also shown in Figs. 4(a)–4(d). Figures 4(a) and 4(b) demonstrate the sharp transition and Figs. 4(c) and 4(d) depict the regime where convective instability occurs displaying the drift of the laminar regime in the turbulent regime and the creation of localised structures. For example, Fig. 4(c) shows the experimentally observed formation of a localised structure near $t = 10ns$ for $n = 220$.

To further characterise the formation of the turbulent puffs, we measured both the intensity and

Optics EXPRESS

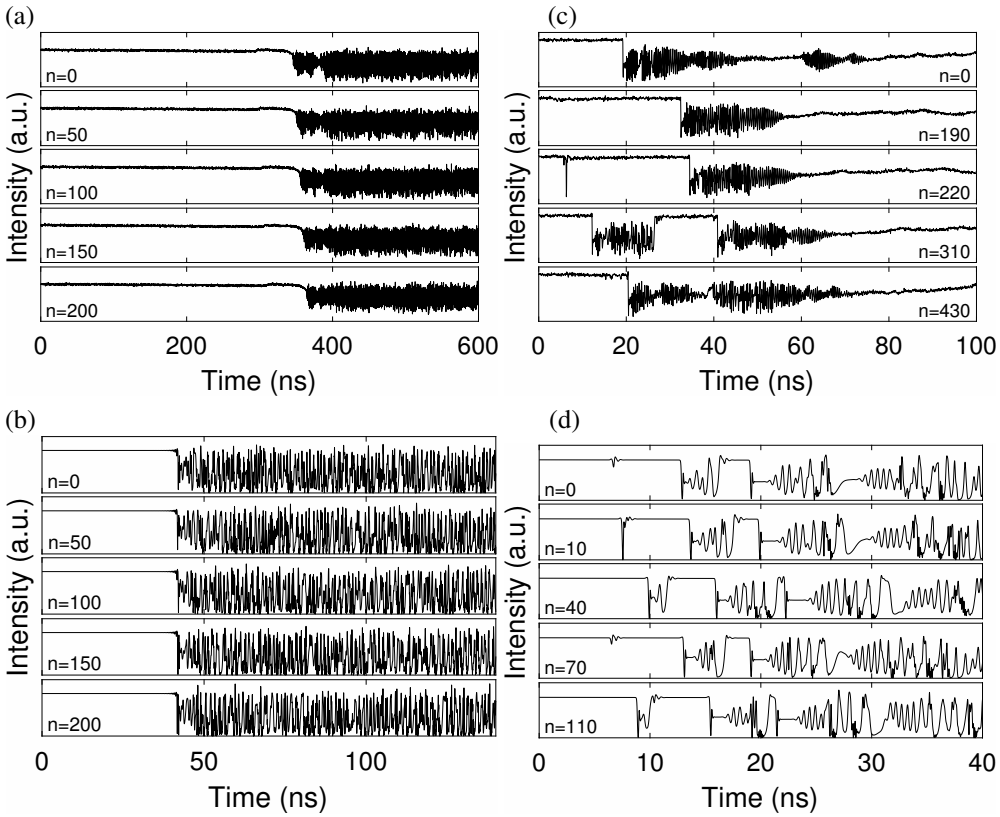

Fig. 4. The detailed analysis of the laser intensity evolution near the subcritical bifurcation point. The laser intensity was recorded at $t = nT_F$, where n is the number of the filter cycles of modulation. Experimental (a) and theoretical (b) observations of the laser intensity demonstrating a sharp transition from laminar to turbulent regimes at a small value of detuning $\delta_{c_1} < \delta < \delta_{c_2}$. This corresponds to the absolute instability regime. The animations of the corresponding regime are shown in Visualisation 1 (experiment) and Visualisation 2 (simulations). Experimental (c) and theoretical (d) observations of creation and drift of turbulent fronts in the convective regime ($\delta_{c_2} < \delta < \delta_{c_3}$). The nucleation of a hole structure that appears suddenly in the cavity is shown in (c) at round trip 220. The animations of the corresponding regime are shown in Visualisation 3 (experiment) and Visualisation 4 (simulations). The parameters for simulations are given in Table 1.

phase of the laser in the initial stage of the creation of these localised structures. To measure the phase, we used the experimental set-up described in [4, 35]. In short, the set-up included a 3x3 self-delayed heterodyne that enabled us to measure the phase difference $\phi(t) - \phi(t - T_d) = \eta(t)$, where T_d is the time difference between the two inputs of the 3x3 coupler. The measurement of the temporal evolution of the laser intensity and phase with a $25ps$ temporal resolution shows that the laser intensity reaches zero with an associated π-phase jump (Fig. 5(a)). Similar results, obtained numerically, are shown in Fig. 5(b). The 2D diagrams of the laser intensity and the associated real part of the electric field are also shown on Fig. 6(b). It is also worthwhile to note that such interferometric technique enabled us to measure the laser linewidth in the various regimes as described in [6]. Using this technique, we observed a coherence collapse at the laminar-turbulent transition where the linewidth on the order of 500MHz in the laminar regime increased to the linewidth of a few GHz in the turbulent regime. This coherence collapse is

another indicator of the growth of turbulence.

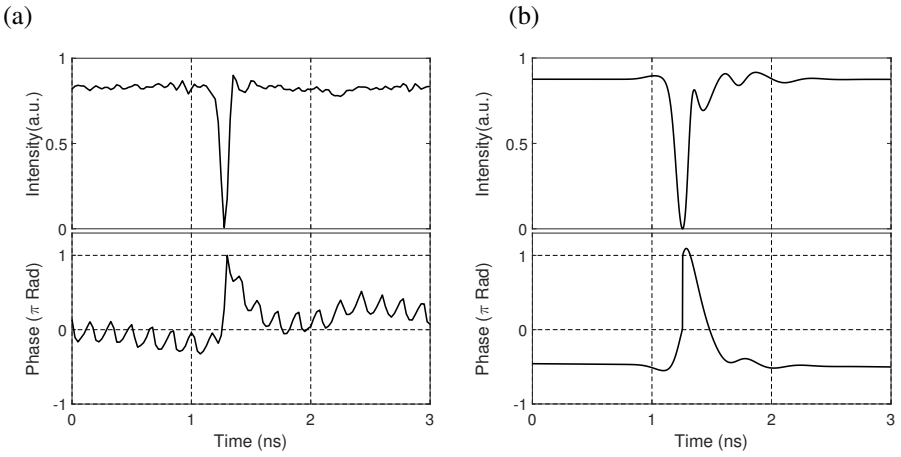

Fig. 5. Experimentally observed (a) and, theoretically modelled (b), temporal evolution of the laser intensity (top) and phase (bottom) during the creation of a localised structure. Note that the laser intensity vanishes while the phase exhibits a π-jump as observed with Nozaki-Bekki holes.

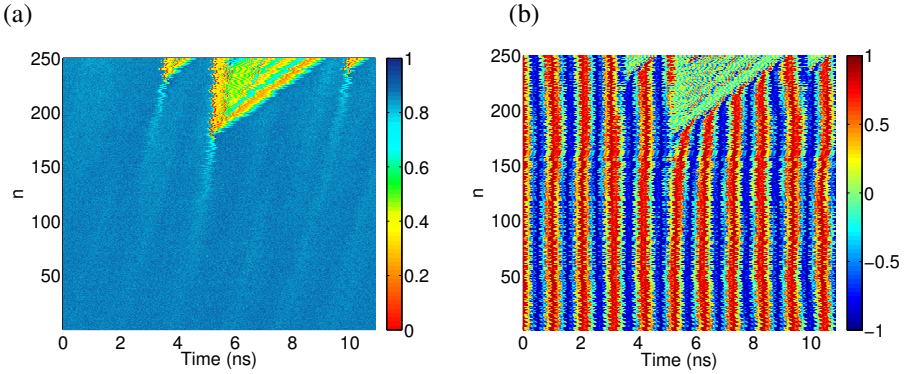

Fig. 6. Creation of three turbulent puffs. Experimentally measured temporal evolution of the laser intensity (a), and real part of the laser field (b) for 250 subsequent filter periods showing the emerging of three Nozaki-Bekki holes that initiate three turbulent regions within the laminar regime.

The observed localised structures (Fig. 5) are similar to the Nozaki-Bekki holes [36, 37] observed in complex Ginzburg-Landau equation. These holes are asymmetric wave sources, emitting different wave numbers up and down streams [38], and it has been suggested that they are the building-blocks of spatio-temporal chaos in convection experiments [39]. In our case, the holes move "downstream" and nucleate the meta-stable turbulent phase that propagates at a larger speed, as demonstrated experimentally and numerically in Figs. 4(c) and 4(d). These turbulent regions grow while drifting and merging with other turbulent regions. As a result, the laminar region continues to invade the turbulent region and other turbulent domains are created.

4. Conclusion

In summary, we have provided, both experimentally and numerically, a scenario for the loss of coherence in a long cavity swept laser. By precisely controlling the detuning between the cavity roundtrip time and the sweep period we were able to demonstrate the transition between an absolute and convective instabilities. In the convective instability regime, we observe a transition to turbulence via creation of convective Nozaki-Bekki holes. This optical analogue of turbulent puffs in hydrodynamics, well-known as Poiseuille flow, reveals the mechanism that leads to deterioration of the coherence of the laser. Delayed differential equations modeling is in excellent qualitative agreement with the experimental observations. It is, to our knowledge, the first experimental observation of Nozaki-Bekki holes inducing the turbulent transition in optical systems.

Funding

Marie Sklodowska-Curie Individual Fellowships European H2020-MSCA-IF-2017, ICOFAS project (800290); Science Foundation Ireland (11/PI/1152); OPTIMAL project granted by the European Union by means of the Fond Européen de développement regional, FEDER; Government of Russian Federation (08-08); Fédération Doeblin CNRS, SFB 787 of the DFG (project B5).

Acknowledgments

The authors thank Stephen Hegarty for help with the experiment and Natalia Rebrova for useful advice and encouraging discussions.

References

1. D. Huang, E. A. Swanson, C. P. Lin, J. S. Schuman, W. G. Stinson, W. Chang, M. R. Hee, T. Flotte, K. Gregory, and C. A. Puliafito, "Optical coherence tomography," Science **254**, 1178–1181 (1991).
2. S. R. Chinn, E. A. Swanson, and J. G. Fujimoto, "Optical coherence tomography using a frequency-tunable optical source," Opt. Lett. **22**, 340–342 (1997).
3. T. Klein and R. Huber, "High-speed oct light sources and systems," Biomed. Opt. Express **8**, 828–859 (2017).
4. T. Butler, S. Slepneva, B. O'Shaughnessy, B. Kelleher, D. Goulding, S. P. Hegarty, H.-C. Lyu, K. Karnowski, M. Wojtkowski, and G. Huyet, "Single shot, time-resolved measurement of the coherence properties of oct swept source lasers," Opt. Lett. **40**, 2277–2280 (2015).
5. M. Bonesi, M. P. Minneman, J. Ensher, B. Zabihian, H. Sattmann, P. Boschert, E. Hoover, R. A. Leitgeb, M. Crawford, and W. Drexler, "Akinetic all-semiconductor programmable swept-source at 1550 nm and 1310 nm with centimeters coherence length," Opt. Express **22**, 2632–2655 (2014).
6. T. P. Butler, S. Slepneva, P. M. McNamara, K. Neuhaus, D. Goulding, M. Leahy, and G. Huyet, "Real-time experimental measurement of swept source vcsel properties relevant to oct imaging," IEEE Photonics J. **9**, 1–10 (2017).
7. D. C. Adler, W. Wieser, F. Trepanier, J. M. Schmitt, and R. A. Huber, "Extended coherence length fourier domain mode locked lasers at 1310 nm," Opt. Express **19**, 20930–20939 (2011).
8. O. Reynolds, "XXIX. An experimental investigation of the circumstances which determine whether the motion of water shall he direct or sinuous, and of the law of resistance in parallel channels," Philos. Transactions Royal Soc. Lond. **174**, 935–982 (1884).
9. K. Avila, D. Moxey, A. de Lozar, M. Avila, D. Barkley, and B. Hof, "The onset of turbulence in pipe flow," Science **333**, 192–196 (2011).
10. J. I. Cardesa, A. Vela-Martín, and J. Jiménez, "The turbulent cascade in five dimensions," Science **357**, 782–784 (2017).
11. D. Castelvecchi, "Mysteries of turbulence unravelled," Nature **548**, 382–383 (2017).
12. P. G. Drazin and W. H. Reid, *Hydrodynamic Stability* (University of Chicago, 1981).
13. L. D. Landau, "On the problem of turbulence," Dokl. Akad. Nauk SSSR **44**, 339–349 (1944).
14. M. C. Cross and P. C. Hohenberg, "Pattern formation outside of equilibrium," Rev. Mod. Phys. **65**, 851–1112 (1993).
15. G. P. Agrawal, "Nonlinear fiber optics," in *Nonlinear Science at the Dawn of the 21st Century,* (Springer, 2000), pp. 195–211.
16. P. Coullet, L. Gil, and F. Rocca, "Optical vortices," Opt. Commun. **73**, 403–408 (1989).
17. I. S. Aranson and L. Kramer, "The world of the complex ginzburg-landau equation," Rev. Mod. Phys. **74**, 99–161 (2002).

Optics EXPRESS

18. E. G. Turitsyna, S. V. Smirnov, S. Sugavanam, N. Tarasov, X. Shu, S. A. Babin, E. V. Podivilov, D. V. Churkin, G. Falkovich, and S. K. Turitsyn, "The laminar–turbulent transition in a fibre laser," Nat. Photonics **7**, 783 (2013).
19. S. Sugavanam, N. Tarasov, S. Wabnitz, and D. V. Churkin, "Ginzburg–landau turbulence in quasi-cw raman fiber lasers," Laser Photonics Rev. **9**, L35–L39 (2015).
20. L. Gao, T. Zhu, S. Wabnitz, Y. Li, X. S. Tang, and Y. L. Cao, "Optical puff mediated laminar-turbulent polarization transition," Opt. Express **26**, 6103–6113 (2018).
21. M. Kolokolnikov, Th.and Nizette, T. Erneux, N. Joly, and S. Bielawski, "The Q-switching instability in passively mode-locked lasers," Phys. D: Nonlinear Phenom. **219**, 13–21 (2006).
22. L. D. Landau and E. M. Lifdhitz, *Fluid Mechanics* (Butterworth-Heinemann, 1987).
23. P. Huerre and P. A. Monkewitz, "Absolute and convective instabilities in free shear layers," J. Fluid Mech. **159**, 151–168 (1985).
24. P. Coullet, T. Frisch, and F. Plaza, "Sources and sinks of wave patterns," Phys. D: Nonlinear Phenom. **62**, 75–79 (1993).
25. A. Couairon and J. M. Chomaz, "Global instability in fully nonlinear systems," Phys. Rev. Lett. **77**, 4015 (1996).
26. R. J. Deissler, "Noise-sustained structure, intermittency, and the ginzburg-landau equation," J. Stat. Phys. **40**, 371–395 (1985).
27. S. Slepneva, B. Kelleher, B. O'Shaughnessy, S. Hegarty, A. G. Vladimirov, and G. Huyet, "Dynamics of Fourier domain mode-locked lasers," Opt. Express **21**, 19240–19251 (2013).
28. R. Huber, M. Wojtkowski, and J. G. Fujimoto, "Fourier domain mode locking (FDML): A new laser operating regime and applications for optical coherence tomography," Opt. Express **14**, 3225–3237 (2006).
29. T. Pfeiffer, M. Petermann, W. Draxinger, C. Jirauschek, and R. Huber, "Ultra low noise fourier domain mode locked laser for high quality megahertz optical coherence tomography," Biomed. Opt. Express **9**, 4130–4148 (2018).
30. C. Jirauschek and R. Huber, "Wavelength shifting of intra-cavity photons: Adiabatic wavelength tuning in rapidly wavelength-swept lasers," Biomed. Opt. Express **6**, 2448–2465 (2015).
31. D. C. Adler, Y. Chen, R. Huber, J. Schmitt, J. Connolly, and J. G. Fujimoto, "Three-dimensional endomicroscopy using optical coherence tomography," Nat. Photonics **1**, 709 (2007).
32. S. Karpf, M. Eibl, W. Wieser, T. Klein, and R. Huber, "A time-encoded technique for fibre-based hyperspectral broadband stimulated raman microscopy," Nat. Comm. **6**, 6784 (2015).
33. C. M. Eigenwillig, W. Wieser, S. Todor, B. R. Biedermann, T. Klein, C. Jirauschek, and R. Huber, "Picosecond pulses from wavelength-swept continuous-wave fourier domain mode-locked lasers," Nat. Comm. **4**, 1848 (2013).
34. G. Giacomelli and A. Politi, "Relationship between delayed and spatially extended dynamical systems," Phys. Rev. Lett. **76**, 2686 (1996).
35. D. Goulding, T. Butler, B. Kelleher, S. Slepneva, S. P. Hegarty, and G. Huyet, "Visualisation of the intensity and phase dynamics of semiconductor lasers via electric field reconstructions," in *Nonlinear Dynamics: Materials, Theory and Experiments,* (Springer, 2016), pp. 3–29.
36. K. Nozaki and N. Bekki, "Exact solutions of the generalized ginzburg-landau equation," J. Phys. Soc. Jpn. **53**, 1581–1582 (1984).
37. N. Bekki and K. Nozaki, "Formations of spatial patterns and holes in the generalized ginzburg-landau equation," Phys. Lett. A **110**, 133–135 (1985).
38. W. van Saarloos and P. C. Hohenberg, "Fronts, pulses, sources and sinks in generalized complex ginzburg-landau equations," Phys. D: Nonlinear Phenom. **56**, 303–367 (1992).
39. J. Burguete, H. Chaté, F. Daviaud, and N. Mukolobwiez, "Bekki-Nozaki amplitude holes in hydrothermal nonlinear waves," Phys. Rev. Lett. **82**, 3252–3255 (1999).